

Article

Not peer-reviewed version

The Uinta Basin Snow Shadow: Impact of Snow-Depth Variation on Winter Ozone Formation

[Michael J Davies](#) , [John R. Lawson](#) ^{*} , [Trevor O'Neil](#) , [Seth N Lyman](#) , KarLee Zager , Tristan D Coxson

Posted Date: 14 August 2025

doi: [10.20944/preprints202508.1019.v1](https://doi.org/10.20944/preprints202508.1019.v1)

Keywords: ozone; air quality; mountain meteorology; snow shadow; precipitation shadow



Preprints.org is a free multidisciplinary platform providing preprint service that is dedicated to making early versions of research outputs permanently available and citable. Preprints posted at Preprints.org appear in Web of Science, Crossref, Google Scholar, Scilit, Europe PMC.

Copyright: This open access article is published under a Creative Commons CC BY 4.0 license, which permit the free download, distribution, and reuse, provided that the author and preprint are cited in any reuse.

Disclaimer/Publisher's Note: The statements, opinions, and data contained in all publications are solely those of the individual author(s) and contributor(s) and not of MDPI and/or the editor(s). MDPI and/or the editor(s) disclaim responsibility for any injury to people or property resulting from any ideas, methods, instructions, or products referred to in the content.

Article

The Uinta Basin Snow Shadow: Impact of Snow-Depth Variation on Winter Ozone Formation

Michael J. Davies ¹, John R. Lawson ^{1,2,*}, Trevor O'Neil ¹, Seth N. Lyman ^{1,3}, KarLee Zager ¹ and Tristan D. Coxson ¹

¹ Bingham Research Center, Utah State University, Vernal, UT 84078, USA

² Department of Mathematics and Statistics, Utah State University, Logan, UT 84322, USA

³ Department of Chemistry and Biochemistry, Utah State University, Logan, UT 84322, USA

* Correspondence: john.lawson@usu.edu

Simple Summary

The authors aim to document a Uinta Basin snow shadow: reduced snowfall in the lee of the Wasatch Mountains. These would change air-quality spatial patterns due to a strong link between ozone concentration and snow depth in winter. We found broad evidence of a shadow in both case studies. However, high uncertainty and low quality of data limits understanding, forecast accuracy, and machine-learning training.

Abstract

After heavy snowfall in the Uinta Basin, Utah, elevated surface ozone occurs when a persistent cold-air pool traps emissions from oil and gas industry operations. Sunlight, assisted by actinic flux from a high-albedo snowpack, drives ozone buildup through photolysis. Snow coverage is paramount to initiate the cold pool and drive ozone generation, hence its depth critical for predicting ozone concentrations. The Basin's location leeward of the Wasatch Mountains provides conditions for a precipitation shadow, where sinking air suppresses snowfall. We analyzed multiple years of ground-based snow depth measurements, surface ozone data, and meteorological observations; we found ozone tracks with snow coverage, but diagnosing a shadow effect (and any impact on ozone levels) was difficult due to sparse, noisy data. The uncertainty in linking snowfall variation to ozone levels hinders forecast quality in, e.g., machine-learning training. We highlight importance of better understanding of regional variation when issuing outlooks to protect local economy and health. Wider sampling of snow depth across the Basin would benefit operational forecasters and, likely, predictive skill.

Keywords: ozone; air quality; mountain meteorology; snow shadow; precipitation shadow

1. Introduction

Episodes of elevated surface ozone concentrations may occur during winter in the Uinta Basin ¹, eastern Utah, USA (Figure 1). These occur when snowfall persists under a temperature inversion for multiple days [1]; i.e., when cold air pools in the Basin, reversing the typical lapse of temperature with height. This inverted thermal setup traps volatile organics ² and nitrogen oxides (NOx) emitted from nearby oil and gas industry [2,3]. Incoming solar radiation is sufficient to drive photolysis but too weak to melt snow sufficiently to counteract nocturnal katabatic winds that fill the Basin with cold, dense drainage flow from the surrounding high terrain [4]. High surface albedo maintains the feedback loop

¹ The spelling *Uinta*—derived from Ute word “pine forest”—refers to geographical features, whereas *Uintah* has been historically used to distinguish use in political and human contexts.

² This nomenclature avoids definitions in terms of volatile organic compounds (i.e., VOCs) due to term's restrictive definition, and instead encompass a large set of compounds crucial to the Uinta Basin system.

by reflecting insolation; critically, this actinic flux extends the path length for photolysis and increases ozone production, resulting in unhealthy air quality that can exceed national U.S. regulatory limits [5]. Despite the importance of snowfall to the Uinta Basin winter-ozone system—as seen in Figure 2 correlating local snow depth and ozone concentration—the influence of terrain on snowfall variation remains poorly understood in part due to difficulty in high-resolution modeling [6] or sparse data in rural areas. Understanding spatial variation in snow depth at the Basin floor is critical for creating improved prediction models or training statistical models [7,8].

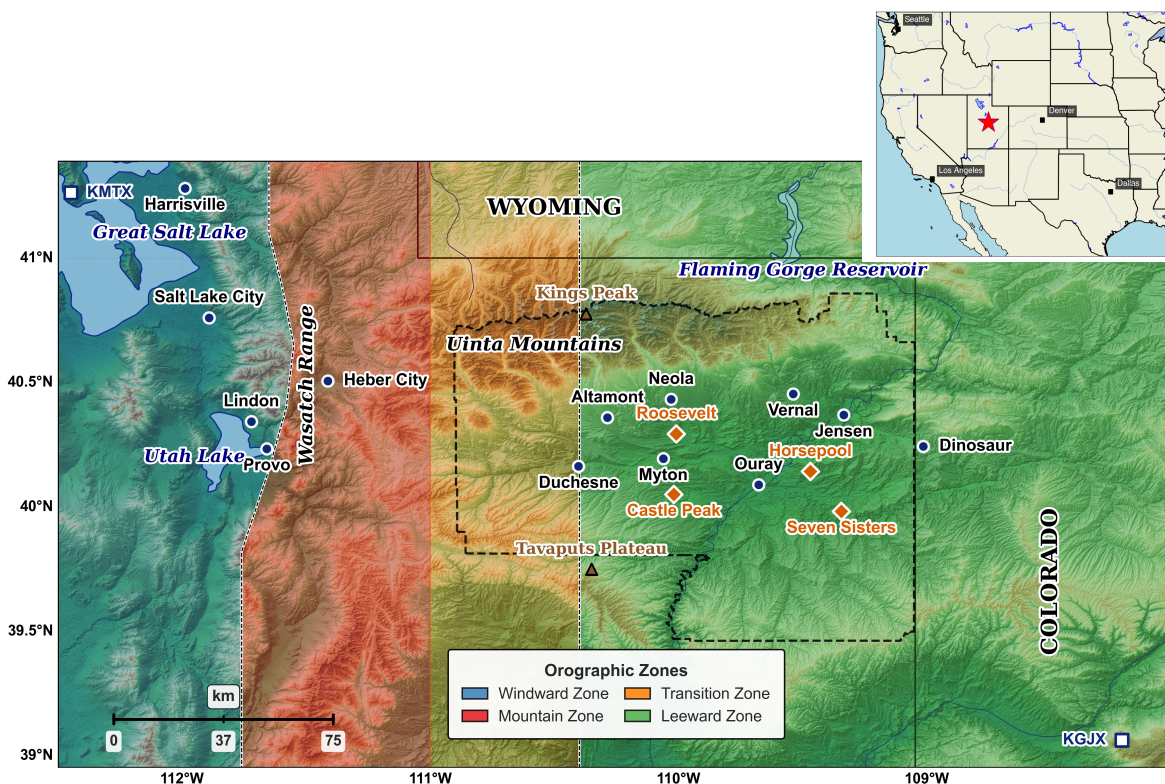


Figure 1. Outline of the two counties in the Uinta Basin, Utah; inset showing location of Utah (red star) in the western continental USA, with select cities for reference marked by black squares. Study area divided into four zones broadly used in the current study with selected cities for reference.

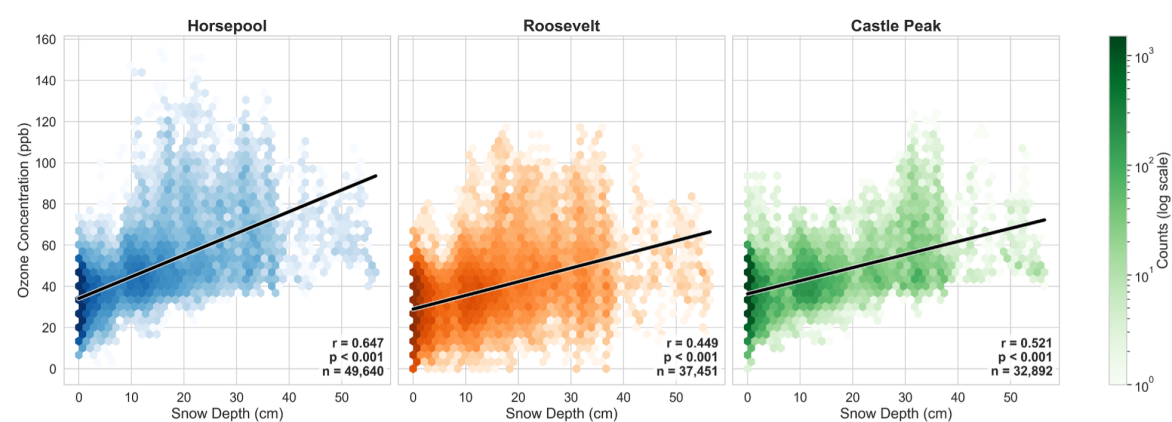


Figure 2. A hexplot that bins observations during winter days in the observation archive for snow depth against ozone concentration. A simple linear fit (black line) shows that snowy days are also more likely to have unhealthy levels of ozone.

Outside of wildfire-driven ozone episodes [9,10] and stratospheric intrusions [11], Uinta Basin ozone episodes are intermittent in their wintertime occurrence [7]. The phenomenon is rare, otherwise documented occasionally in, e.g., similar mountainous basins with oil and gas operations such as the

Upper Green River Basin near Pinedale, Wyoming [12], and northern [13] and eastern China [14,15]. Ozone is more familiar as a summertime problem due to intense sunshine and more anthropogenic pollution sources in cities like Los Angeles [16], Beijing [17], Salt Lake City [18], etc. Elevated levels may also occur in rural areas with summertime oil and gas industrial emissions [19]. Health studies link elevated ozone levels with added respiratory stress, particularly for sensitive groups with conditions like asthma [20–22]. Regulatory responses in the USA are within purview of the Environmental Protection Agency (EPA) which set the National Ambient Air Quality Standards (NAAQS) threshold at 70 ppb for ozone. Predicting elevated levels of ozone is important for both public health and protecting the local economy from sanctions and economic ramifications. Multiple days of high ozone concentrations can trigger *non-attainment designations* and limits on industry operations. Hence, better understanding is in the interest of all stakeholders and the public [23], not only of scientific interest.

However, predicting air quality is a challenge in mountainous regions [24,25], in part due to complex interactions between atmospheric flow and orographic features [26, pp.327–334]. Subsequent mechanisms (mountain waves, adiabatic effects, etc.) perturb windward flow characteristics and dictate many features on the leeward microclimate [27]. One such phenomenon, the *precipitation shadow effect*, is seen as increasing rain- or snowfall as one moves further leeward of a mountain range [24] that are typically “more complex than the textbook explanation” [28]. It is defined by the American Meteorological Society as “...a region of sharply reduced precipitation on the lee side of an orographic barrier.”[29] The current study studies snowfall, but most documented cases involve variations in rainfall. At the foundation, both phenomena occur through the same mechanism:

1. Moist flow encounters higher terrain and is forced upward
2. Rising air parcels cool, and resulting condensed water liquid precipitates predominately on the windward side
3. This process depletes air parcels of moisture
4. When drier air descends on the leeward side, it warms adiabatically, further taking the air parcels from saturation; hence, less moisture is available for precipitation
5. Subsiding, dry air creates a “shadow” of reduced snowfall or rainfall.

Strong adiabatic warming (i.e., from compression under gravity) can cause a *föhn effect* [30] on the leeward side that can cause maximum dry-bulb temperatures that exceed those at locations typically warmer (e.g., [31]). This warming can lead to the “snow-eater” effect seen in, e.g., the European Alps [24,32], where snow-melt is limited to the mountain crest wake. Warming drying winds can also exacerbate wildfire risks such as in destructive Santa Ana/Los Angeles events in the southwestern U.S. [33–35]. Further, the sensitivity of snow depth to snow-water equivalent and humidity (e.g., sublimation) are further uncertainties that gives the prediction of snow depth challenges not seen in rain shadows.

Regional studies, e.g., Mansfield [7, p.1] state as self-evident that a snow shadow exists in the Basin; however, the authors are not aware of formal documentation or quantification of a Uinta Basin snow shadow. The present study gauges evidence of this received wisdom, especially given the importance of snowfall for initiating the winter-ozone feedback loop. Observations of meteorological and air-quality parameters are critical for the Basin’s ozone warning program [8,23], both in nowcasting (i.e., real-time monitoring of observations) and forecast-model optimization (whether evaluation or machine-learning training). We restrict our focus to snowfall events with predominantly westerly flow at Wasatch crest height, due to its prevailing frequency and association with textbook snow-bearing storms [36]. We identify several important gaps that limit our understanding of spatial variation of snow depth in the Uinta Basin, and hence winter ozone formation:

1. **Do we find evidence of a Uinta Basin snow shadow?** This would appear as less snow in the lee of the Wasatch than on the windward slopes, the challenge of a fair comparison in varying terrain notwithstanding;

2. **Do we see an impact of spatial snowfall variations on ozone levels?** A greater extent of snow coverage would provide conditions associated with unhealthy build-up of ozone. If less snow falls in the western extent of the Basin, does this restrict ozone levels?;
3. **How certain are our data in rural, complex terrain?** High uncertainty reduces the rigor of prediction, evaluation, and conceptual models. Data from *in situ* meteorological and chemistry sensors is sparse in comparison to urban regions, and Doppler radar data poorly samples the Basin. This is inherent noise.

We begin by reviewing pertinent studies that progressively link the meteorological impact of snow-depth variation on air chemistry and ozone formation.

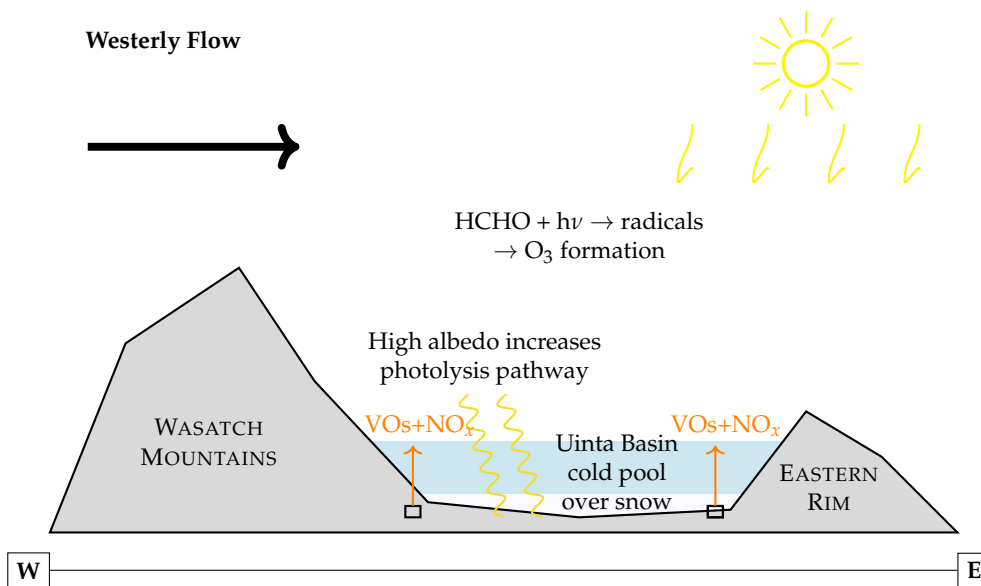


Figure 3. Schematic of a west–east cross-section through the Uinta Basin (cf. Fig. 1, where W and E in the diagram denote approximately Provo to Dinosaur, respectively) depicting the winter-ozone formation mechanism. The persistent cold pool maintains snow cover (and hence high albedo), increasing the path length for photolytic reactions to act on pollutants trapped within the cold pool. Volatile organics are abbreviated as VO_s.

2. Background

The rarity of elevated wintertime surface ozone stems from the need to balance multiple factors before winter ozone can be reliably generated:

- Equatorward enough to receive sufficient sunlight for photolysis
- Poleward enough to preserve snow (less insolation and lower temperatures)
- The higher the elevation, the stronger the insolation
- Complex terrain cold-pool formation in mountain valleys and basins
- Precursors to ozone (i.e., volatile organics; NO_x)

Precursor emissions are provided mostly by oil and gas industry operations. The high elevation also means background levels—even without human influence—are higher due to natural seepage and stratospheric intrusion of ozone-rich air. Snow-bearing weather systems generally move with a west-to-east component, though sensitivity of snowfall to wind direction in Utah [37] is outside the scope of the current study.

We consider two windstorm subtypes. So-called Wasatch windstorms [38,39] occur in easterly flow north of the Uinta Mountains (Figure 1). Flow blocked by the west–east Uinta Mountains is funneled towards lower surface pressure in Salt Lake City. When easterlies cross the Wasatch Range, windstorms can occur in Davis County (Figure 1), gusts measured as exceeding 46 m s⁻¹ (102 mph; 89 kt). Air does not warm: the descending wind is similar to a waterfall [38]: a pooling of cold air behind (east of) the crest that spills over the crest (Figure 1).

Conversely, further south, westerly flow crossing the Wasatch into the Uinta Basin has a steeper rise-and-fall for moist airflow to navigate. During (north-)westerlies, air is forced to rise from ~1300 m (4250 ft) to ~3500 m at Wasatch crest-level (this results in the self-described “Greatest Snow On Earth” [40]). Drier air parcels then descend into the Heber Valley (~1700 m), or continue over terrain exceeding 3000 m (9800 ft) between Heber City and Duchesne (~1700 m) (cf. terrain in Figures 1 and 3). Thus, understanding flow in complex: will the flow descend into the Heber Valley (this may depend on atmospheric stability)? Now in our area of interest, flow descends to the Basin’s lowest point ~1400 m (4600 ft) near Ouray (Figure 1) and ascends gradually to a ~2500 m plateau east of the Utah–Colorado border. Completing the bowl-like terrain pattern, the pre-Cambrian Uinta Range bound the Basin to the north at 3500–4000 m; the Book and Roan Cliffs (generally, the Tavaputs Plateau) likewise at ~3000 m to the south.

Ozone episodes are most frequent in the second half of winter [7], whose higher solar angles in February balance thermal disruption to persistent cold pools. While much work cited herein identifies the connections between snowfall and ozone production, it does not fully quantify impacts of spatial patterns. The sparse network of snowfall observations in the region provides a challenge towards this endeavor. A lack of reliable data also hinders the development of predictive tools at short and long temporal ranges. Continuously reliable data is fundamental to training machine learning and AI-based models for winter air-quality prediction [e.g., 8,41].

Stockham et al. [27] found a standard definition of rain shadows can lack important local distinctions, e.g., Peak District, UK. Representative timescales and physical mechanisms vary with latitude, season, etc. Rain shadows occurred much less frequently than hypothesized: fewer than 1 in 5 days with prevailing wind conditions. Representative of numerical prediction as a whole, Ghan et al. [42] found climate models may struggle to capture precipitation shadows, consistently showing “too little precipitation on the windward side” and *vice versa*: their models could not reproduce “sub-grid rain shadows”; i.e., a suppression of precipitation occurring at scales below that which the model can capture (i.e., the scale of truncation).

Even in the absence of complex topography, snow accumulation can be highly spatially variable. Snow depth is sensitive to numerous mechanisms and surface characteristics, including sublimation, melting, refreezing, settling, vegetation type, soil temperature, and the lofting and drifting of snow. The reported depth of snow is modulated by wind-driven sublimation [43, p. 189], potentially relevant given the long fetch along the Basin’s longest axis. Modeling evaporation and sublimation from a Basin snow coverage can lead to unrealistic snow depth values [44, p. 2423], adding to uncertainty from surface roughness (friction). Further, drifting and settling in varying terrain degrades representivity of snow reports. Estimation of melt is reliable [45], but errors in soil temperature and intermittent melt-freeze sequences can accumulate and not capture marginal freezing cases [46], degrade snow-water equivalent estimates [47], etc. Compacting snow makes the pack denser but shallower [48].

It is unknown to what magnitude these variations impact ozone concentration. Yet despite the challenges identified in conducting robust studies, snow shadows were documented in Maine, USA in 1942 [49], while Kusaka et al. [50] documented an unorthodox snow shadow on the Sea of Japan coast, displaying parallels with US mountain phenomena [51] including involving seas or lakes [52].

3. Data and Methods

We recapitulate our main aim of exploring our observation dataset to determine whether there is the signature of a snow shadow mechanism, as defined above.

3.1. Study Area

Figure 1 shows broad regions used herein, chosen during initial work and for reference to areas in text. Stations that are listed as active in the Synoptic Weather data repository are plotted in Figure 4 with their station ID to highlight the contrast in the amount of snow-depth observations between the Wasatch Front and Uinta Basin (cf. terrain in Figure 1). Stations prefixed with “COOP” are volunteer-run National Oceans and Atmospheric Administration (NOAA) Cooperative Stations

(<https://www.weather.gov/coop/overview>, accessed 1 June 2025) that report snow-depth manually once-daily with precision to the nearest 1 in (2.5 cm). This coarse sampling in time, space, and precision poses an obstacle to finer, robust snow-depth measurement, especially in the western part of the Basin leeward of the highest terrain (near Duchesne in Figs. 1 and 4).

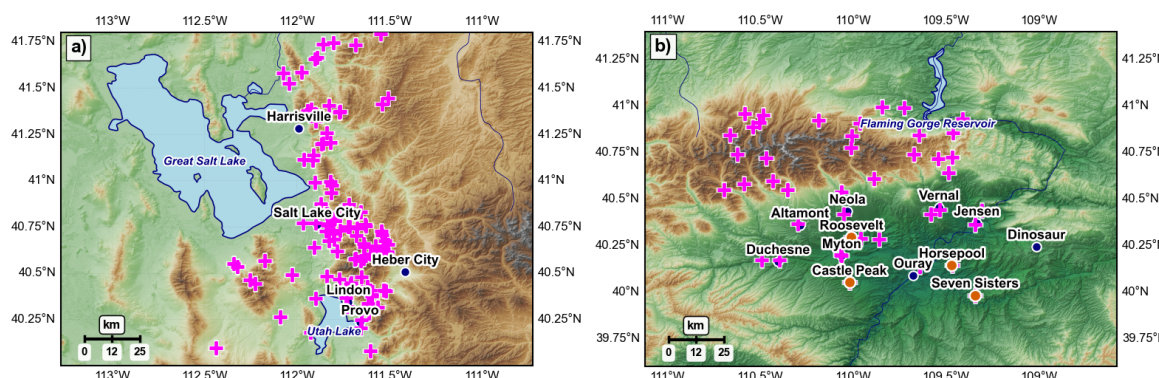


Figure 4. Stations reporting snow depth in the Synoptic Weather database (all those ever marked ‘active’), locations marked with magenta cross. Towns labeled with black squares for reference in later discussion. (Also see Figure 1).

3.2. Cases and Data

Observation data is less reliable in complex terrain than flatter landscapes due to the low representivity of stations and poor spatial/temporal sampling. Further, observational noise is not consistent between stations: at least one station operated by the Bingham Research Center was manually corrected for animal interference, for example, while we identified another site prone to drifting near the sensor. Preliminary work revealed periods of unreliable data: measurement gaps, obviously spurious outliers, and limited spatial coverage to increase confidence of observation fidelity. We acquired NOAA GOES-satellite visible-channel imagery from the repository at <https://www.star.nesdis.noaa.gov/goes/index.php> to complement *in situ* observations for a basic yes/no for snow coverage in the our study areas (Figure 1).

3.3. Data Collection

Utility of satellite is restricted by its infrequent sampling of the Basin (once or twice daily) and frequent cloud cover during times where information on snowfall is most useful. Further, there are few intersections of the relatively low frequency of satellite passes ($\approx 1 \text{ day}^{-1}$) and winter storm systems that bear $\geq 75\text{mm}$ snow for the Basin ($\approx 2 \text{ month}^{-1}$) required to trigger the feedback loop for ozone production (Figure 3).

Other satellite data relevant to the present topic [53,54], such as albedo or low-level lapse rates, are outside the current scope but have found limited success in preliminary work due to large uncertainty.

3.3.1. Doppler Radar

The Basin’s distance from the closest Doppler radars—part of the U.S. national radar network (NEXRAD)—limits detection of Basin precipitation due to terrain beam-blocking. Radar sites at Grand Junction (KGJX) and Salt Lake City/Promontory Point (KMTX) [55, their Figure 1] can overshoot falling precipitation: as the beam radiates from the radome in a conical manner, a beam must be high enough to clear the Basin’s circumferential terrain but low enough to sample below cloud base. Resultant estimates of precipitation amounts are less reliable than, for instance, the downstream Great Plains region [56, p. 2035]. In summer, cloud bases in the high desert can reach $\sim 4 \text{ km AGL}$, meaning rain or hail may be detected on radar, but evaporation and/or sublimation of the precipitation shaft (i.e., *virga*) would occur undetected below the lowest possible beam (i.e., 0.2°). This would result in an overestimation of rainfall. Conversely, shallow Basin winter cold pools are $O(100 \text{ m})$ [1,25]. This would result in underestimation of snowfall due to overshooting of the lowest radar beam. Due to the

importance of radar coverage for predicting conditions for ozone formation, we inspect the sampling regions more closely by computing the lowest height of a radar beam above the Basin from the two radars in proximity (Figure 5). Beams blocked by terrain are masked with a black pixel and colored pixels show the minimum height above ground level. The figure reveals how poorly that precipitation detection could behave, particularly in the west and central parts of the Basin. (The mathematics of our computation is presented in Appendix A). The same problem of overshooting radar beams is documented elsewhere, including the windward Wasatch slopes as sampled from KMTX ([36]their Figure 2)

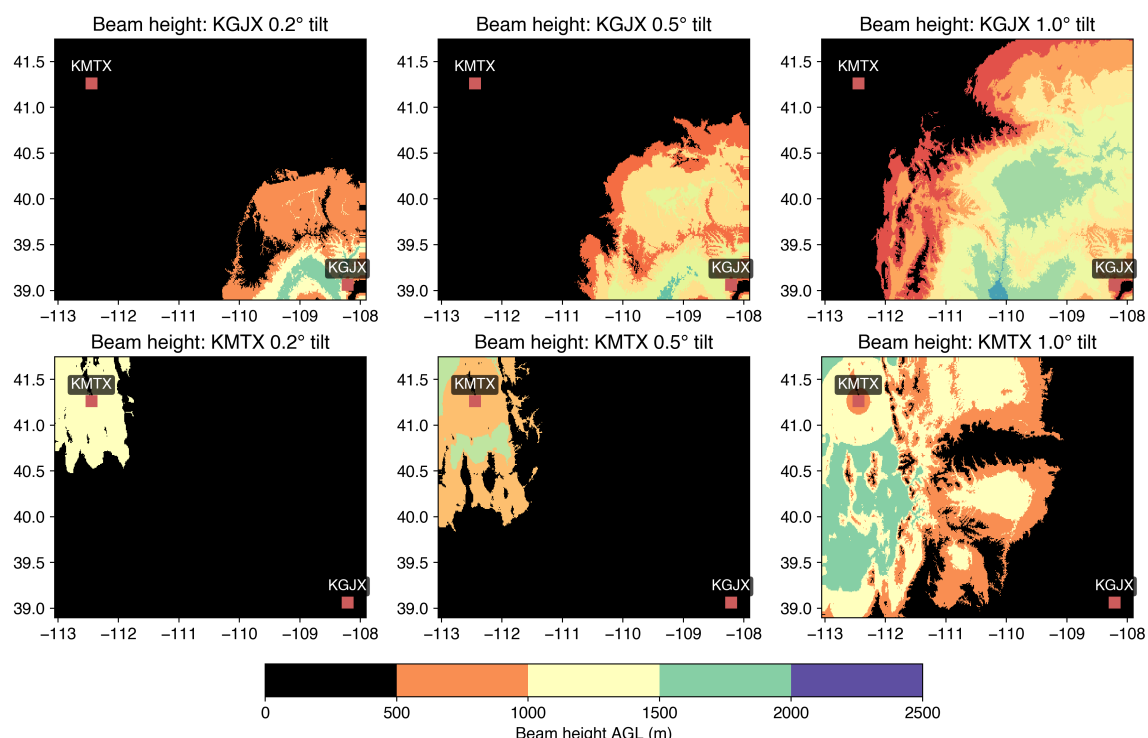


Figure 5. Height above ground level (AGL) of the lowest three radar-beam tilts from Grand Junction (top three; KGJX) and Salt Lake City (bottom three; KMTX). NEXRAD radar locations are at the bottom right (KGJX) and top left (KMTX). The calculations shown are tilt angle at 0.2° , 0.5° , and 1.0° . The lowest 0.2° angle is permitted for these two sites [e.g., 55] but is evidently of little use to the Basin (located center-right in each frame). Black pixels indicate blocked radar beams from either radar site.

To summarize: regions where this surface significantly exceeds Basin-floor elevations indicate poor radar sampling of precipitation due to blocking by the surrounding high terrain and inherent curvature upwards of the conical beam. Eastern parts of the Basin (near Vernal) are mostly sampled due to their line of sight to KGJX rather than KMTX blocked by the taller Wasatch Range. This creates high uncertainty for live viewers of radar data regarding precipitation reaching the surface (hence, so too the hydrometeor type). We see the signature of a so-called "radar hole" in later precipitation radar-derived estimates.

3.3.2. In Situ Meteorological Sensors

We obtain 20 years of archived data from Synoptic Weather repositories (<https://synopticdata.com/national-mesonet-program/>, accessed 1 January 2025), part of the U.S. National Mesonet Program. All sites reporting snow depth in our period of record and zones of interest are shown in Figure 4. The Bingham Research Center further deploys its own stations (those marked in red on Figure 4 maps) as part of its air quality network (UBAIR). Raw data is sent from the field site via cellular internet to Synoptic Weather repository archives almost immediately; however, multiple sources of error

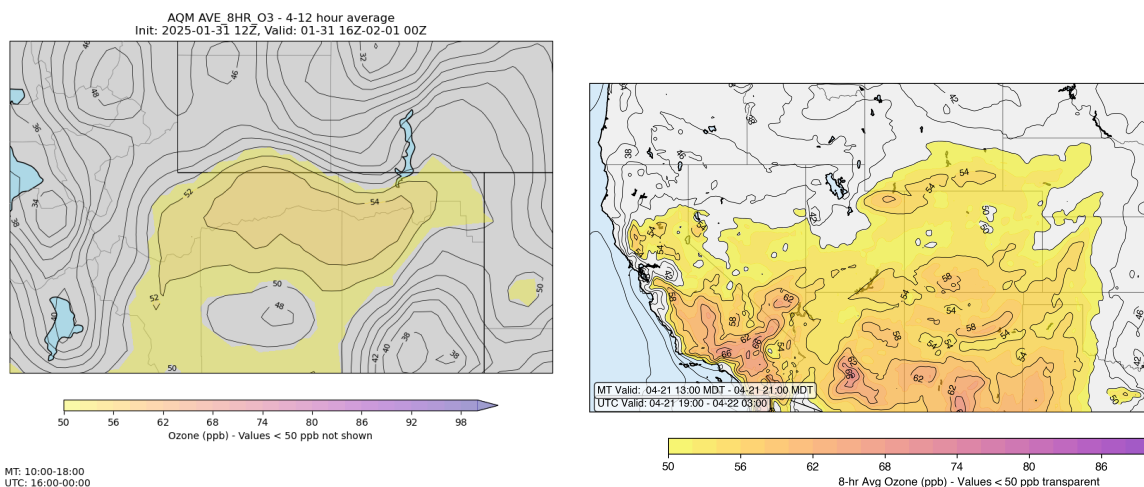
(e.g., drifting; animal interference; thermal contraction) necessitates careful postprocessing. Further automating this error correction method is an ongoing effort to improve availability of snow data for purposes of ozone forecasting.

Ozone concentrations were not necessarily sampled at the same site as snow depth but site choice heavily accounted for suitable coherence between both observations' insight into the real state. The generalization of measured ozone concentration is uncertain and likely flow-dependent due to non-constant emission inventories across the Basin (e.g., oil and gas rigs opening in new locations, while old sites close). The changes are slow enough to enable skillful training of AI-based ozone predictions [8], but it remains difficult to anticipate step changes in industry operations, and hence ozone precursors.

3.3.3. Numerical Weather Prediction Model Data

The national Air Quality Model (AQM), part of the next generation of NOAA NWP systems (the Unified Prediction System), can miss high-ozone events due to the small scale of the Basin and coarse resolution of AQM. For instance, a high ozone event on Jan 31 2025 was not captured by AQM forecasts (Figure 6a), while high ozone associated with wildfires in the U.S. Southwest were larger scale and within the purview of AQM simulation (Figure 6b). This inability of traditional NWP models to adequately capture both uncertainty and fine-scale airflow motivated the direct statistical prediction of ozone using fuzzy logic inference to drive the Bingham Research Center's yearly Ozone Alert program, where stakeholders receive periodic email about potential elevated-ozone episodes. Thousands of lightweight simulations can be performed for the cost of one traditional simulation that may be precise and detailed, but not necessarily accurate and physically realistic: indeed, our observation network is too coarse to verify the fine scales of up- and down-canyon flow simulated in a high-resolution numerical experiment, for example.

We also deploy analyses from the High-Resolution Rapid Refresh (HRRR) model as a proxy for gridded "truth", i.e., forecast hour 0. We primarily inspect two analysis products to supplement observations of snow: its depth and spatial coverage.



(a) Forecast of surface ozone initialized 31 Jan 2025, hours 4–12: coarse AQM model missed the > 70 ppb event in southcentral Basin.

(b) Forecast 8-hour average surface ozone for hours 15–23, initialized 21 Apr 2025; captures stratospheric intrusion with elevated ozone across SW.

Figure 6. Illustrative example of the dependence of AQM ozone forecast skill on season, due to the shallow nature of cold-air pools in the Basin and the coarse grid spacing of AQM. The charts display maximum 8-hour averaged surface ozone concentration, taken from the NOAA AQM model. The first case was associated with a persistent, shallow cold pool enabling > 70 ppb measurements in the south-central Basin—this is not captured by the coarse AQM model; the latter was tentatively associated with large scale processes, likely stemming from an intrusion of stratospheric, ozone-rich air in tandem with wildfire season expanding across North America.

3.3.4. Precipitation Estimates: RTMA

It is understandably difficult to estimate precipitation amounts in complex terrain due to low representativity of stations, large variability in conditions, and sparsity of observations in remote areas. To supplement raw in situ observations, the Real-Time Mesoscale Analysis (RTMA) system was developed by the National Centers for Environmental Prediction (NCEP) to create more continuous maps of, e.g., precipitation across the USA at 5-km horizontal grid-spacing [57]. The system uses two-dimensional variational data assimilation (2DVAR), where the Jacobian (linearized observation operator) adjusts a prior model state towards an optimal combination of weather observations and model analyses, representing a best guess. Originally, RTMA ingested Rapid Update Cycle model forecasts down-scaled from 13-km to 5-km horizontal grid-spacing as background fields; later, the system incorporated HRRR backgrounds that improved analysis quality further [58].

Given our interest in air quality correlated with mountain meteorology, we note methods in RTMA that include terrain-following techniques designed to account for complex orography, e.g., anisotropic background error covariances that follow terrain gradients [57]. However, limitations remain outside of flat terrain [58] such as in Utah within the U.S. Intermountain West [57, their Figure 8]: some RTMA products displayed no skill in the West over raw observations. These shortcomings were acknowledged, including issues with quality control and optimization for cases in small-scale valleys and basins. Tyndall and Horel [59] found disproportionate impacts from mountainous stations and rail-network sensors in remote locations such as central-east Utah, including the Uinta Basin. Accordingly, more advanced systems are required to capture high-complexity flow using, e.g., flow-dependent covariance matrices [60], though even advanced methods performed poorly in sloping terrain and elevations above ~1 km—typical of Utah’s ranges and basins [61].

For quantitative precipitation estimates (QPE), RTMA ingests Doppler radar data from the NEXRAD WSR-88D national network operated by the National Weather Service. De Pondeca et al. [57] explain how radar data are combined with rain gauge information as Stage II analyses further compared and detailed in [62, and refs. therein]. However, in regions such as the Uinta Basin with

poor radar coverage (Figure 5) and sparse *in situ* observations (Figure 4), the existing high-terrain issue of poor representivity and unreliable optimization schemes is compounded further. Accordingly, we maintain a focus on trustworthiness of RTMA data in the Basin.

3.4. Filtering and Post-Processing

The sparse network of snowfall observations in the region makes it difficult to study these effects, creating challenges for both understand the underlying processes and developing predictive tools. Data obtained from Synoptic Weather have quality control, but nonetheless, we still need to apply more post-processing where data gaps are not substantial (i.e., not representative in time; over ~3 hours). We identified outliers in snow depth measurements from weather stations across the Uinta Basin, Utah. The errors were mostly sudden spikes that diverging from recognizable snow-depth series. We recognize that outliers result from sensor malfunctions, transmission errors, or genuine environmental conditions. We also determine the error characteristics of the site of interest and sensitivity to local conditions or terrain.

We must choose a filter that is balanced: extremes must be handled carefully to avoid squashing events important to our air-quality context. Further, and with unavoidable subjectivity, the processing should not fabricate large windows in time from which we infer results. In preliminary testing, we found the *Hampel filter* [63, and refs. therein] most effective when evaluated subjectively by eye. It was less likely to smooth out extreme values in preliminary testing than other filters, and was robust when the chosen window was small enough to preserve persistent snowfall. The filter operates by sub-setting a sliding window of size $2m$, computing median-absolute-deviation (MAD) to identify outliers, and replacing them with a subset median if they exceed a multiple n of the MAD. The drawback of the Hampel filter is degraded performance in symmetric Gaussian-noise regimes. Ultimately, its best subjective performance justified use of the Hampel method to filter snowfall time series used herein. We do not filter the COOP network (i.e., once-daily quantized at 2.54 cm intervals). The group will deploy the above filtering method on time series shown on the Research Center's experimental Basin air-quality portal at www.basinwx.com.

4. Results

Reiterating our goals, we review multiple sources of data—observations, RTMA, reanalyses—to quantify any association between snow depth and distance from the Wasatch, and whether elevated ozone patterns correspond to those in snow coverage. For reader reference, the study area begins winter in UTC-7 and moves to UTC-6 by its conclusion.

Case 1: Late February 2023

In the first half of this case, elevated ozone occurred in the Basin (Figure 7). Snow depth during this time was sufficient in the Basin (Figure 8) to allow buildup of ozone.

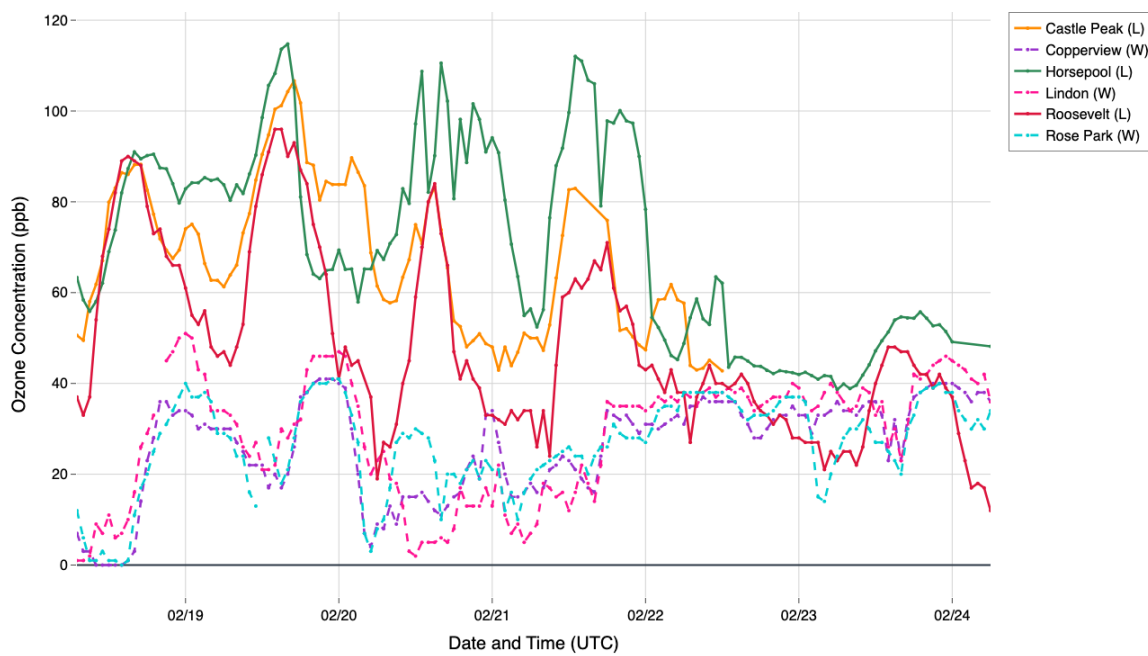


Figure 7. Ozone concentration measured on the windward (Copperview; Lindon; Rose Park) and leeward/Basin (Castle Peak; Horsepool; Roosevelt) side of the Wasatch Mountains for the period 0600 UTC 18 February to 0600 UTC 24 February 2023. Simulated snow cover is shown in Figure 9 during this period.

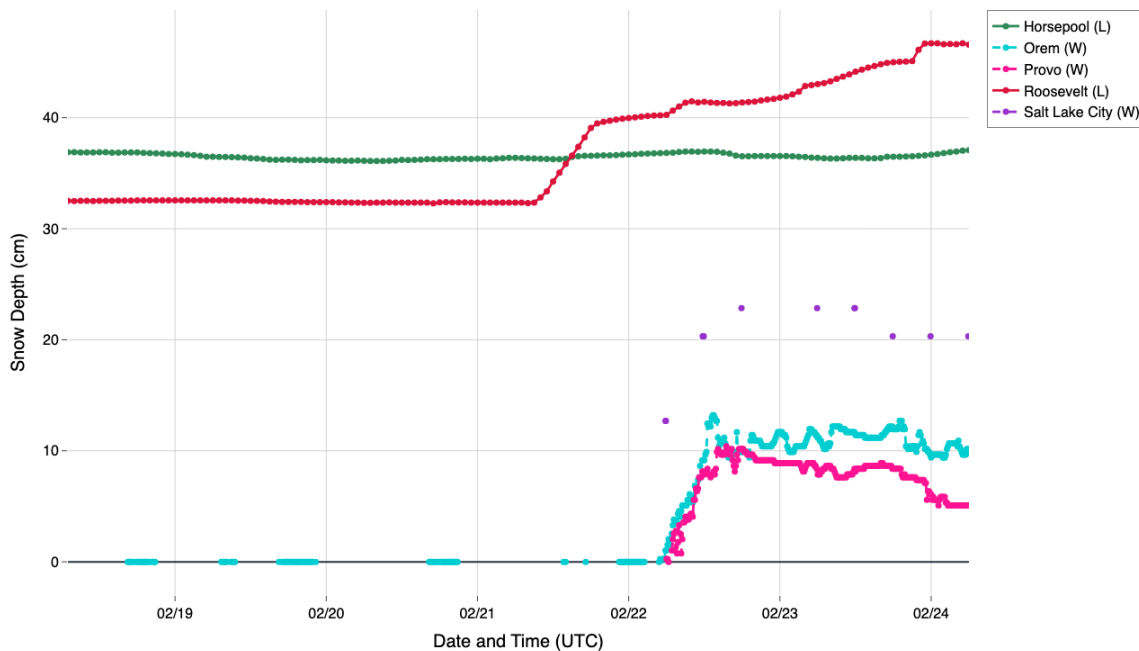


Figure 8. Snow depth measured on the windward (Orem; Provo) and leeward/Basin (Castle Peak; Horsepool; Roosevelt) side of the Wasatch Mountains for the same period as in Figure 7.

The early snow was captured in the HRRR analyses broadly correctly (Figure 9) but at a shallow depth, potentially related to lack of radar detection, sampling by satellite, weather observation station data, etc. Nonetheless, there is suggestion of less snowfall (a snow shadow) in observed data for the snow passage round 23 February (contrast the two site groups in Figure 8).

HRRR Snow Analysis
Valid: 2023-02-22 12:00 UTC

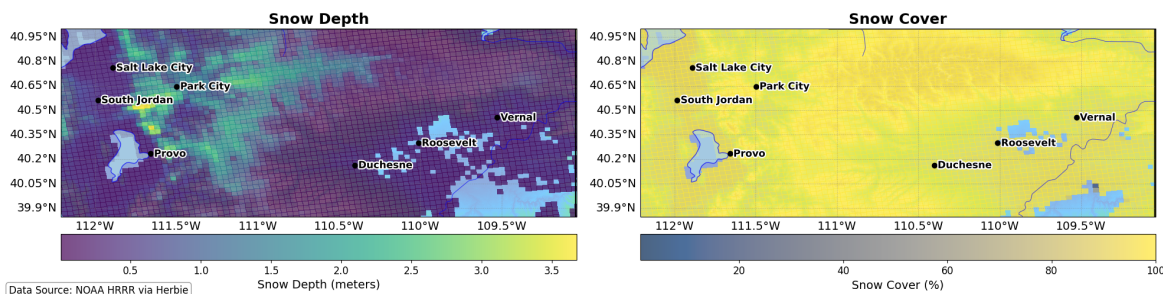


Figure 9. Snow depth (cm) and cover (percent area) from High Resolution Rapid Refresh (HRRR) model analysis (forecast time zero), 1200 UTC 22 February 2023.

Relating this to the larger context, we see that a snow shadow, should it exist, is not reducing snowfall coverage to an amount that precludes ozone buildup. Perhaps it reduces the probability a cold pool will form, all else assumed constant; further exploration is outside the scope of the current study.

We derived an estimate of total storm accumulation (or liquid equivalent, if snow) adding 6 days' totals per grid point in RTMA data. Evidently, the estimated accumulated precipitation product from RTMA (Figure 10), hence did not detect snowfall during the week with a critical snow-pack: moreover, the radar "hole" is evident in near-zero accumulations for the Basin despite observed snowfall (implied by satellite imagery in Figure 12). The precipitation product in Figure 10 and at other times (not shown) often display a brighter band emanating from the radar location, marking a region (e.g., crest level) where beams pass unobstructed until reaching the hydrometeor of interest.

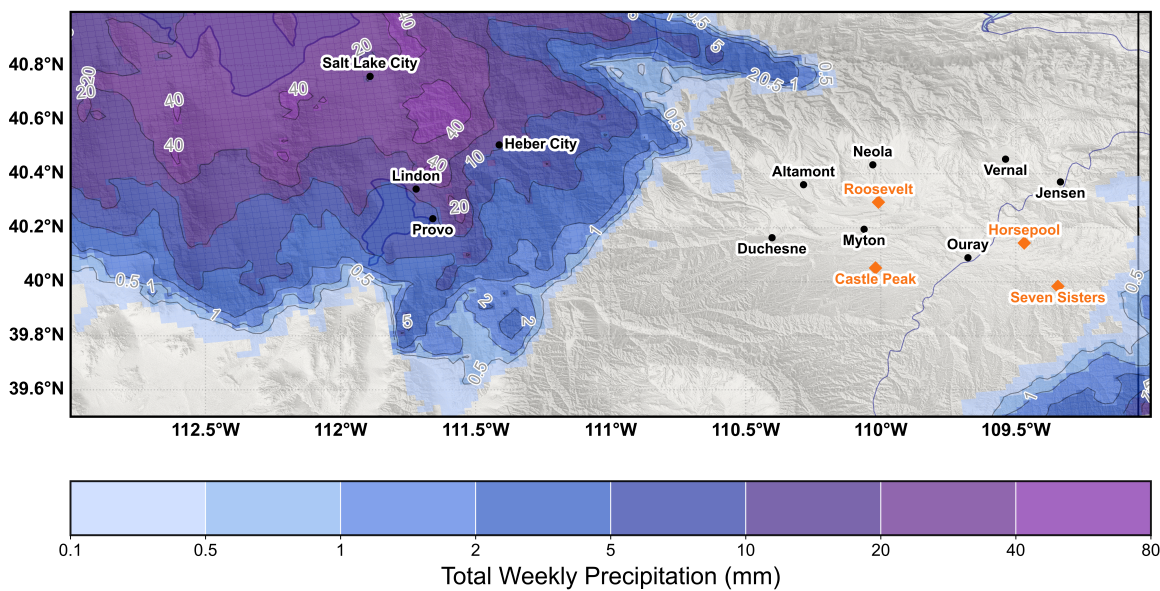


Figure 10. Total storm precipitation (snow-water equivalent if frozen) from the RTMA gridded observation product valid roughly at the end of the study period. Snow was observed on both sides of the Wasatch Range but RTMA is unaware of much that fell across the Uinta Basin (cf. Figure 1).

The gross underestimate of snowfall in the Basin likely stems from under-sampling when terrain blocks Doppler radar (cf. Figure 5) and not remedied by incorporation of sparse rain-gauge data when producing the Stage II gridded QPE product. Indeed, the RTMA product's use of radar data is conspicuous by its prominent striping.

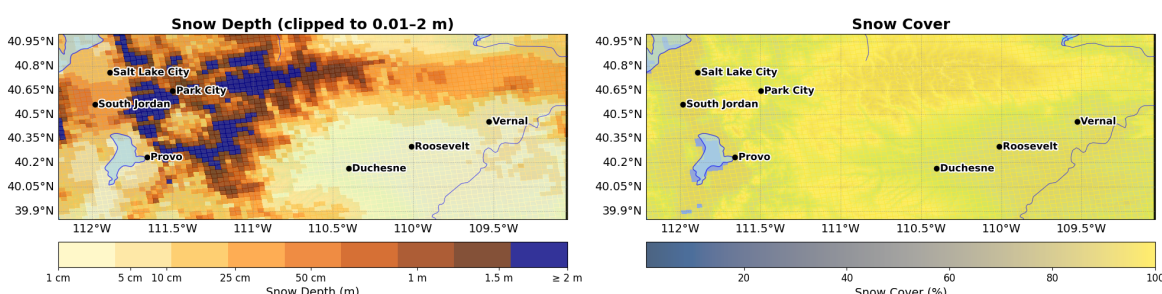


Figure 11. HRRR analyses, similar to those in Figure 9, but valid 1200 UTC, 24 February 2023.

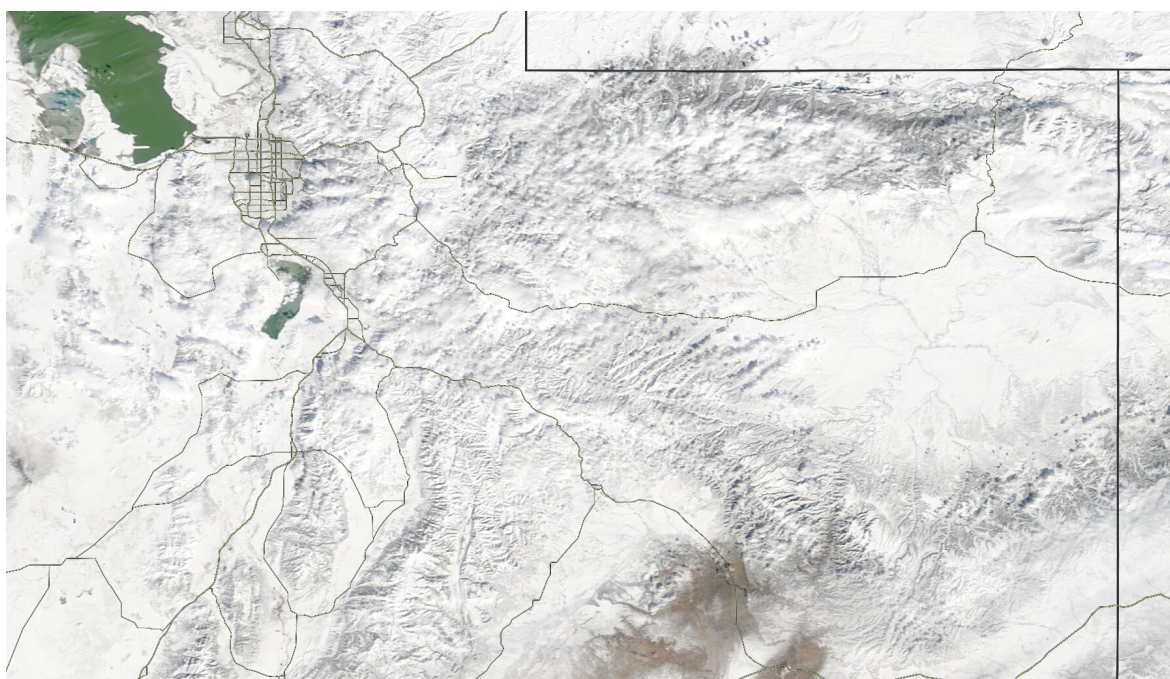


Figure 12. Visible satellite image (MODIS Terra), valid 2203 UTC, 24 February 2023, showing snow throughout the Uinta Basin.

Analysis of the February 2023 episode reveals mixed evidence for snow shadow effects. While satellite imagery (Figure 12) shows widespread snow coverage across the Basin, RTMA precipitation estimates (Figure 10) failed to detect snowfall in the western Basin during the 22–28 February period, likely due to radar beam blocking rather than actual precipitation differences. This creates an artifact that presents similarly (but erroneously) as a snow shadow. Ozone concentrations (Figure 7) reached 70–100 ppb in Basin locations while remaining around 40 ppb on the Wasatch Front, consistent with the winter ozone formation mechanism requiring persistent snow cover and trapped precursors. The episode demonstrates that even modest snow accumulations can sustain ozone episodes when combined with stable atmospheric conditions shown in Figure 3. Contributions to ozone concentration from factors additional to spatial variation of snow depth (e.g., elevation; proximity to industry operations) may be inextricable and preclude more certain diagnoses.

Case 2: 27 January 2025

The January 2025 case provides better RTMA–observation agreement, with HRRR analyses (Figure 13) capturing both snow depth and coverage patterns visible in satellite imagery (Figure 14). Snow depths show gradual increase from west to east across the Basin floor, potentially indicating shadow effects, though it is difficult to corroborate in observations. Basin ozone concentrations touched the 70 ppb threshold during this episode (not shown), with peak values correlating spatially with areas of persistent snow cover identified in both model analyses and satellite data. These are supporting

signs of a connection between spatial heterogeneity and ozone concentration, but do not robustly diagnose a snow shadow explicitly.

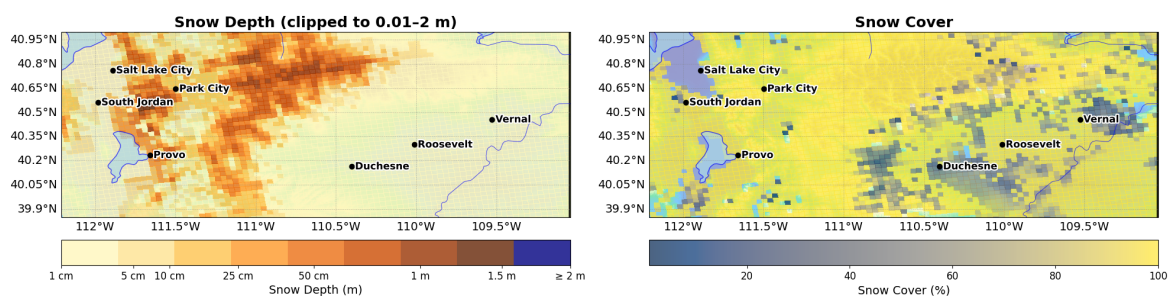


Figure 13. An analysis of snow depth and coverage at 0000 UTC on 27 January 2025.

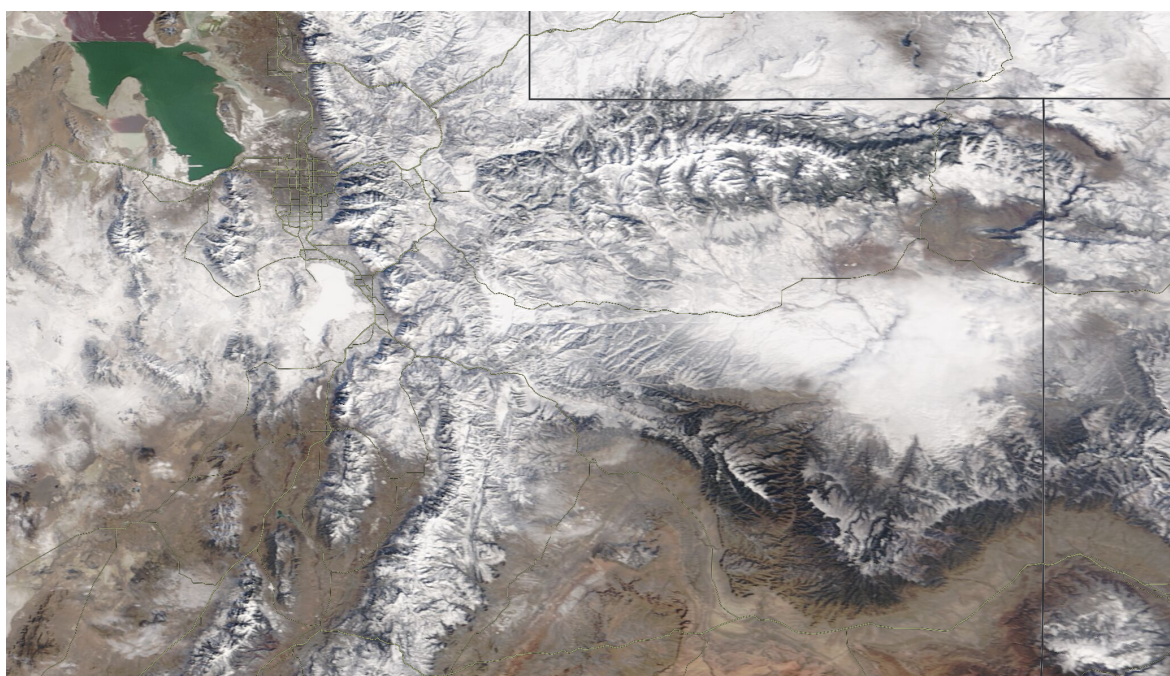


Figure 14. Visible satellite image (MODIS Terra), valid 2203 UTC, 27 January 2025, showing snow coverage across the study region.

Surface dry-bulb and dew-point temperatures (Figure 15) display a wider-scale drying that more holistically explains a reduction in precipitation Basin-wide, albeit not in the lee of the higher terrain. Conceptually, weather effectively passes over the Basin—especially so during stable winter episodes that reinforce over a snow pack—and this may track with a lack of documented windstorms or damage in the lee of surrounding terrain.

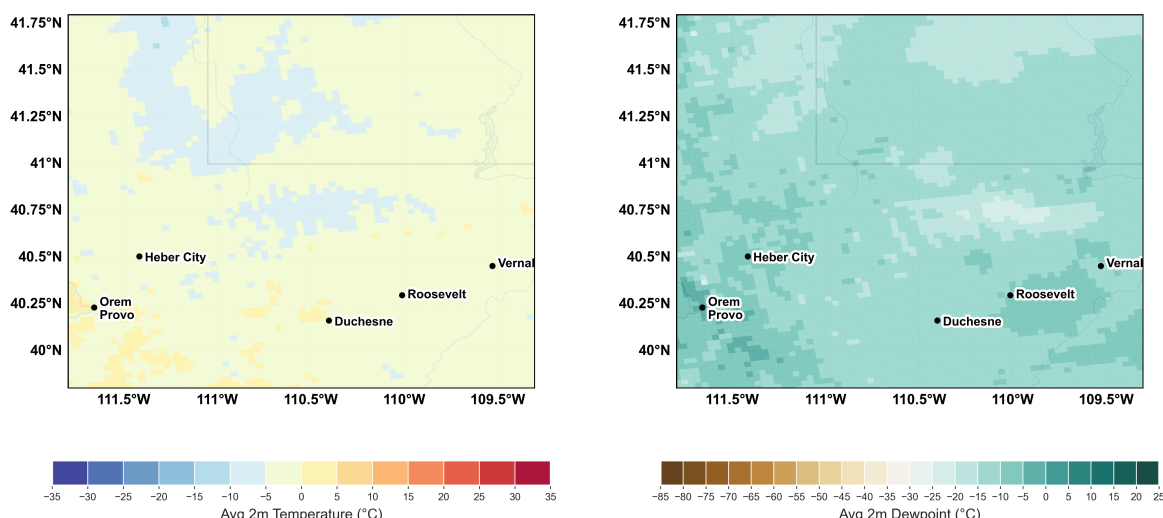


Figure 15. HRRR analyses, valid 1200 UTC, 27 January 2025, showing (a) 2-m dry-bulb (a) and dew-point (b) temperatures.

Our analysis faced significant challenges in documenting snow shadow effects and air quality implications. While qualitative evidence supported some elements of our initial science questions, quantitative confirmation is hindered by: (1) radar beam blocking that creates artificial precipitation holes in gridded products; (2) sparse *in situ* observations that inadequately sample spatial gradients; and (3) complex terrain that confounds windward–leeward comparisons. Despite observational limitations, connections emerge between snow coverage and ozone formation. As in many other cases documented in Lyman et al. [64] and similar annual reports before it, episodes with widespread Basin snow coverage produce elevated ozone concentrations exceeding 70 ppb when other conditions allow (stable, high pressure; sufficient insolation), while periods with patchy or absent snow typically show near-background ozone levels regardless of precursor emissions. This reminds operational forecasters of the critical role in albedo for maintaining ozone-producing boundary layers (Figure 3).

5. Conclusions

We set out to address three key questions regarding snow shadows and winter ozone formation in the Uinta Basin:

Do we find evidence of a Uinta Basin snow shadow? Broadly, yes. While the mathematical theory and historical observations suggest reduced precipitation leeward of the Wasatch Mountains, data-quality limitations prevent definitive confirmation. RTMA precipitation estimates are unreliable due to radar coverage gaps, and while it appears to show a clear snow-shadow pattern in our case studies (and other preliminary work), this is likely an artifact of sparse near-surface radar data. Surface observations are too sparse for robust spatial analysis. However, satellite corroborated HRRR numerical estimates of snow coverage, and the Perhaps this is unsurprising due to its lower elevation; fair comparison of different elevations remains an open question.

Do we see an impact of spatial snowfall variations on ozone levels? Yes: in the first case (e.g., Figure 7), Basin stations sampled high ozone daily maxima (i.e., over 70 ppb) absent along the Wasatch Front (windward); regional connections may exist between snow coverage extent and ozone concentrations, but elevation (cold pool strength) and contributions to high ozone from proximity to industry are also inextricable factors. Fine-scale impacts of precipitation gradients on ozone spatial patterns remain difficult to quantify, partly due to a small sample size.

How certain are our data in rural, complex terrain? Uncertainty is substantial and limits predictive and diagnostic capability. Radar beam blocking creates systematic gaps in precipitation monitoring; sparse surface networks inadequately capture spatial gradients; uncertainty hampers the accuracy of our alert communications for industry regulatory compliance and public health.

There are unique challenges of predicting elevated winter ozone in the Uinta Basin, Utah, USA. Primarily, the dependence of ozone formation on sufficient snow depth necessitates good knowledge of the current state for both nowcasting and initiating numerical prediction of high-ozone episodes. In the authors' experience, it is received wisdom in the local community that the Basin lies in a snow shadow: a region with lower snowfall accumulations close in the lee of the crest but increasing depth as one moves further leeward. The lower humidity and typical snowfall levels is quickly evident, corroborating an accepted truth. However, during the course of increasing the rigor of a snow-shadow diagnosis, and subsequent impact on ozone formation and prediction, relatively low data quality (sparsity; representivity; sampling frequency or consistency) hampered more robust assessments of precipitation estimates due to factors including radar-beam blocking, a sparse observation network, and infrequent satellite passes.

Some adjacent takeaway points include:

- Poor estimates of precipitation accumulation from RTMA is insufficiently corrected by a sparse network of radar and *in situ* observations;
- In summer, cloud base may be 1–2 km AGL; hence beams can sample precipitation that may evaporate or sublimate between this level and the surface (*virga*), resulting in overestimation from radar returns
- In winter, cloud bases are within the lowest kilometer, meaning any precipitation is unlikely to be sampled despite lower likelihood of *virga* from the shorter, colder path to the surface

While it is less important to label a phenomenon with as many caveats as outlined above, understanding sources of observation and model error is paramount to improve training of machine-learning or artificial-intelligence models.

High uncertainty should motivate larger, coarser ensembles (of traditional or AI sorted alike), rather than running at finer resolutions. In balance, vertical grid spacing must be fine enough to capture a shallow cold pool in a traditional NWP model. It is the curse of dimensionality, however, that prevents the evaluator from knowing if the complexity is *precision rather than accuracy*.

5.1. Future Work

Research avenues slated for ongoing and future investigation include:

- Data analysis over a longer time period;
- Low-cost snow-depth sensors [e.g., 65] over a wide area, reporting live on the COOP network;
- Analysis of ozone concentration and snowfall amounts for weather systems with different pre-vailing wind directions;
- Identification of new observation sites that would most benefit ozone and snow prediction [e.g., 66];
- Methods to extract information (despite trends in industry operations and snowfall intermittency) with further statistical processing [67].

Artificial Intelligence statement

The authors used the following large-language models during the course of the research, but no generated text output was used verbatim in the manuscript, and all output was fact-checked by the authors. For lower-complexity use-cases, we used DeepSeek R1 1776, an uncensored instance of the open-sourced DeepSeek package hosted by Perplexity in the United States. On top of good performance, a motivation for use of DeepSeek R1 1776 over, e.g., traditional web searches was its lower energy footprint based on author estimates.

OpenAI GPT o4-mini-high	Python coding assistance
OpenAI GPT o3	Research brainstorming
OpenAI Codex	LaTeX typesetting fixes
Claude Opus 4.0	Python visualization assistance
DeepSeek R1 1776	Information collation

Author Contributions: Conceptualization, MJD and JRL; methodology, MJD, JRL, SNL, and TN; software, MJD, JRL, SNL, TN, TDC, and KZ; validation, MJD and JRL; formal analysis, MJD and JRL; fitting metrics, JRL; investigation, MJD, JRL, SNL, TN, TDC, and KZ; resources, SNL; data curation, MJD, JRL, SNL, TN, TDC, and KZ; writing—original draft preparation, MJD and JRL; writing—review and editing, MJD, JRL, SNL, TN, TDC, and KZ; visualization, MJD and JRL; supervision, SNL and JRL; project administration, JRL; funding acquisition, SNL. All authors have read and agreed to the published version of the manuscript.

Funding: This work was funded by *Uintah County Special Service District 1* and the Utah Legislature.

Data Availability Statement: Code used herein is available in repositories hosted at www.github.com/bingham-research-center, comprising python functions and worked Jupyter notebooks. Much of this development is and was assisted by generative AI output from GitHub Copilot A.I. and other large-language models listed above. Operational products improved by the current work are hosted at www.basinwx.com, operated by the Bingham Research Center.

Acknowledgments: The authors thank Alex Jacques at Synoptic Weather and John Horel at the University of Utah for work in sending our group's observations to the Synoptic Weather repository; non-credited co-authors at the Bingham Research Center for their assistance with apparatus and data collection; Brian Blaylock for continued maintenance of key python packages *SynopticPy* and *Herbie*; Pamela Gardner for reviewing an earlier draft of the manuscript; local insight and initial conversation with Tracie Kingsford.

Conflicts of Interest: The authors declare no conflicts of interest.

Abbreviations

The following abbreviations are used in this manuscript:

NOx	Nitrogen oxides
BRG	Bingham Research center
KVEL	Vernal Regional Airport
KSLC	Salt Lake International Airport
NOAA	National Oceans and Atmospheric Agency
UFS	Unified Forecasting System
NEXRAD	Next Generation Radar?
HRRR	High Resolution Rapid Refresh (model)
AQM	Air Quality Model (NOAA UFS)
AGL	Above Ground Level

Appendix A.

Computation of radar-beam height and terrain blocking We first obtained high-resolution Digital Elevation Model (DEM) data covering the Uinta Basin. We use the USGS ~10 m grid downsampled to a grid with spacing of 1°-by-1°designed for computational efficiency. The DEM ranges over a bounding box extending from the Salt Lake City (KMTX) and Grand Junction (KGJX) radars (top left and bottom right, respectively, in the six Figure 5 panels.

Grid Definition

We define a regular grid of longitude–latitude points

$$\{(\lambda_i, \phi_j) : \lambda_{\min} \leq \lambda_i \leq \lambda_{\max}, \phi_{\min} \leq \phi_j \leq \phi_{\max}\} \quad (\text{A1})$$

with spacings $\Delta\lambda$, $\Delta\phi$ chosen so that the horizontal cell-size $\Delta x \approx R_e \cos \phi \Delta\lambda$ does not exceed the vertical resolution requirements of the beam-width footprint at maximum range [68].

For each grid point (λ_i, ϕ_j) and for each radar site (λ_r, ϕ_r) we compute the slant range r_{ij} using the spherical-Earth approximation:

$$r_{ij} = R_e \arccos(\sin \phi_r \sin \phi_j + \cos \phi_r \cos \phi_j \cos(\lambda_i - \lambda_r)), \quad (\text{A2})$$

where $R_e \approx 6.371 \times 10^6$ m is the assumed mean Earth radius.

Beam Height Computation

At each slant range r_{ij} we compute the beam height above mean sea level for the lowest elevation tilt θ (0.2° for KMTX and KGJX in low-level elevation mode):

$$h_{ij} = h_r + r_{ij} \sin \theta + \frac{r_{ij}^2}{2 R_e}, \quad (\text{A3})$$

where h_r is the radar site elevation. The first term accounts for the site height, the second for the linear beam rise, and the third for Earth's curvature (rationale taken from National Weather Service recommendations for correcting beam bending correction at https://www.weather.gov/media/lsx/wcm/decision/RadarTraining_2010.pdf, accessed 1 May 2025.)

Let T_{ij} denote the terrain elevation from the DEM at grid cell (i, j) . We define clearance

$$\Delta h_{ij} = h_{ij} - T_{ij}. \quad (\text{A4})$$

A grid cell is not masked (visible) if $\Delta h_{ij} > 0$, and blocked otherwise. For each cell we can record the minimum sampling height

$$h_{\min, ij} = \begin{cases} h_{ij}, & \Delta h_{ij} > 0, \\ \infty, & \Delta h_{ij} \leq 0, \end{cases} \quad (\text{A5})$$

and optionally take the point-wise minimum over both radars:

$$h_{\min, ij}^{(\text{combined})} = \min(h_{\min, ij}^{(\text{KMTX})}, h_{\min, ij}^{(\text{KGJX})}). \quad (\text{A6})$$

but results from this computation were used in analysis and not shown herein.

References

1. Neemann, E.M.; Crosman, E.T.; Horel, J.D.; Avey, L. Simulations of a cold-air pool associated with elevated wintertime ozone in the Uintah Basin, Utah. *Atmos. Chem. Phys.* **2015**, *15*, 135–151. <https://doi.org/10.5194/acp-15-135-2015>.
2. Lyman, S.; Tran, T. Inversion structure and winter ozone distribution in the Uintah Basin, Utah, U.S.A. *Atmos. Environ.* **2015**, *123*, 156–165. <https://doi.org/10.1016/j.atmosenv.2015.10.067>.
3. Schnell, R.C.; Oltmans, S.J.; Neely, R.R.; Endres, M.S.; Molenar, J.V.; White, A.B. Rapid photochemical production of ozone at high concentrations in a rural site during winter. *Nat. Geosci.* **2009**, *2*, 120–122. <https://doi.org/10.1038/ngeo415>.
4. Schnell, R.C.; Johnson, B.J.; Oltmans, S.J.; Cullis, P.; Sterling, C.; Hall, E.; Jordan, A.; Helmig, D.; Petron, G.; Ahmadov, R.; et al. Quantifying wintertime boundary layer ozone production from frequent profile measurements in the Uinta Basin, UT, oil and gas region. *J. Geophys. Res.* **2016**, *121*. <https://doi.org/10.1002/2016jd025130>.
5. Edwards, P.M.; Brown, S.S.; Roberts, J.M.; Ahmadov, R.; Banta, R.M.; deGouw, J.A.; Dubé, W.P.; Field, R.A.; Flynn, J.H.; Gilman, J.B.; et al. High winter ozone pollution from carbonyl photolysis in an oil and gas basin. *Nature* **2014**, *514*, 351–354. <https://doi.org/10.1038/nature13767>.
6. Jones, C.; Tran, H.; Tran, T.; Lyman, S. Assimilating satellite-derived snow cover and albedo data to improve 3-D weather and photochemical models. *Atmosphere (Basel)* **2024**, *15*, 954. <https://doi.org/10.3390/atmos15080954>.

7. Mansfield, M.L. Statistical analysis of winter ozone exceedances in the Uintah Basin, Utah, USA. *J. Air Waste Manag. Assoc.* **2018**, *68*, 403–414. <https://doi.org/10.1080/10962247.2017.1339646>.
8. Lawson, J.R.; Lyman, S.N. A preliminary fuzzy inference system for predicting atmospheric ozone in an intermountain basin. *Air* **2024**, *2*, 337–361. <https://doi.org/10.3390/air2030020>.
9. Xu, L.; Crounse, J.D.; Vasquez, K.T.; Allen, H.; Wennberg, P.O.; Bourgeois, I.; Brown, S.S.; Campuzano-Jost, P.; Coggon, M.M.; Crawford, J.H.; et al. Ozone chemistry in western U.S. wildfire plumes. *Sci. Adv.* **2021**, *7*, eabl3648. <https://doi.org/10.1126/sciadv.abl3648>.
10. Jaffe, D.A.; Wigder, N.L. Ozone production from wildfires: A critical review. *Atmos. Environ. (1994)* **2012**, *51*, 1–10. <https://doi.org/10.1016/j.atmosenv.2011.11.063>.
11. Lin, M.; Fiore, A.M.; Cooper, O.R.; Horowitz, L.W.; Langford, A.O.; Levy, H.; Johnson, B.J.; Naik, V.; Oltmans, S.J.; Senff, C.J. Springtime high surface ozone events over the western United States: Quantifying the role of stratospheric intrusions. *Journal of Geophysical Research: Atmospheres* **2012**, *117*. <https://doi.org/10.1029/2012JD018151>.
12. Mansfield, M.L.; Hall, C.F. A survey of valleys and basins of the western United States for the capacity to produce winter ozone. *J. Air Waste Manag. Assoc.* **2018**, *68*, 909–919. <https://doi.org/10.1080/10962247.2018.1454356>.
13. Tang, G.; Wang, Y.; Li, X.; Ji, D.; Hsu, S.; Goa, X. Spatial-temporal variations in surface ozone in Northern China as observed during 2009–2010 and possible implications for future air quality control strategies. *Atmospheric Chemistry and Physics* **2012**, *12*.
14. Li, G.; Bei, N.; Cao, J.; Wu, J.; Long, X.; Feng, T.; others. Widespread and persistent ozone pollution in eastern China during the non-winter season of 2015: observations and source attributions. *Atmospheric Chemistry and Physics* **2017**, *17*.
15. Li, K.; Jacob, D.J.; Liao, H.; Qiu, Y.; Shen, L.; Zhai, S.; Bates, K.H.; Sulprizio, M.P.; Song, S.; Lu, X.; et al. Ozone pollution in the North China Plain spreading into the late-winter haze season. *Proc. Natl. Acad. Sci. U. S. A.* **2021**, *118*. <https://doi.org/10.1073/pnas.2015797118>.
16. Peterson, J.; Demerjian, K. The sensitivity of computed ozone concentrations to U.V. radiation in the Los Angeles area. *Atmospheric Environment* **1976**, *10*, 459–468. [https://doi.org/10.1016/0004-6981\(76\)90026-3](https://doi.org/10.1016/0004-6981(76)90026-3).
17. He, H.; Li, Z.; Dickerson, R.R. Ozone pollution in the North China Plain during the 2016 Air Chemistry Research in Asia (ARIAs) campaign: Observations and a modeling study. *Air (Basel)* **2024**, *2*, 178–208. <https://doi.org/10.3390/air2020011>.
18. Jaffe, D.A.; Ninneman, M.; Nguyen, L.; Lee, H.; Hu, L.; Ketcherside, D.; Jin, L.; Cope, E.; Lyman, S.; Jones, C.; et al. Key results from the salt lake regional smoke, ozone and aerosol study (SAMOZA). *J. Air Waste Manage. Assoc.* **2024**. <https://doi.org/10.1080/10962247.2024.2301956>.
19. Marsavin, A.; Pan, D.; Pollack, I.B.; Zhou, Y.; Sullivan, A.P.; Naimie, L.E.; Benedict, K.B.; Juncosa Calahoranno, J.F.; Fischer, E.V.; Prenni, A.J.; et al. Summertime ozone production at Carlsbad caverns National Park, New Mexico: Influence of oil and natural gas development. *J. Geophys. Res.* **2024**, *129*. <https://doi.org/10.1029/2024jd040877>.
20. Balmes, J.R. The role of ozone exposure in the epidemiology of asthma. *Environ. Health Perspect.* **1993**, *101 Suppl 4*, 219–224. <https://doi.org/10.1289/ehp.93101s4219>.
21. McConnell, R.; Berhane, K.; Gilliland, F.; London, S.J.; Islam, T.; Gauderman, W.J.; Avol, E.; Margolis, H.G.; Peters, J.M. Asthma in exercising children exposed to ozone: a cohort study. *Lancet* **2002**, *359*, 386–391. [https://doi.org/10.1016/S0140-6736\(02\)07597-9](https://doi.org/10.1016/S0140-6736(02)07597-9).
22. Zu, K.; Shi, L.; Prueitt, R.L.; Liu, X.; Goodman, J.E. Critical review of long-term ozone exposure and asthma development. *Inhal. Toxicol.* **2018**, *30*, 99–113. <https://doi.org/10.1080/08958378.2018.1455772>.
23. Bingham Research Center.; Lawson, J.R. 2023 Annual Report: Bingham Research Center, 2023. <https://doi.org/10.5281/ZENODO.13999275>.
24. Whiteman, C.D. *Mountain Meteorology: Fundamentals and Applications*; Oxford University Press, USA, 2000; p. 355.
25. Tran, T.; Tran, H.; Mansfield, M.; Lyman, S.; Crosman, E. Four dimensional data assimilation (FDDA) impacts on WRF performance in simulating inversion layer structure and distributions of CMAQ-simulated winter ozone concentrations in Uintah Basin. *Atmos. Environ. (1994)* **2018**, *177*, 75–92. <https://doi.org/10.1016/j.atmosenv.2018.01.012>.
26. Markowski, P.; Richardson, Y. *Mesoscale Meteorology in Mid-latitudes*; Wiley-Blackwell, 2010; p. 407.
27. Stockham, A.J.; Schultz, D.M.; Fairman, J.G.; Draude, A.P. Quantifying the Rain-Shadow Effect: Results from the Peak District, British Isles. *Bull. Am. Meteorol. Soc.* **2017**. <https://doi.org/10.1175/BAMS-D-17-0256.1>.

28. Van den Hende, C.; Van Schaeybroeck, B.; Nyssen, J.; Van Vooren, S.; Van Ginderachter, M.; Termonia, P. Analysis of rain-shadows in the Ethiopian Mountains using climatological model data. *Clim. Dyn.* **2021**, *56*, 1663–1679. <https://doi.org/10.1007/s00382-020-05554-2>.

29. American Meteorological Society. *Rain shadow*, 2024.

30. Hoinka, K.P.; Tafferner, A.; Weber, L. The ‘miraculous’ föhn in Bavaria of January 1704. *Weather* **2009**, *64*, 9–14. <https://doi.org/10.1002/wea.251>.

31. Bennie, J.J.; Wiltshire, A.J.; Joyce, A.N.; Clark, D.; Lloyd, A.R.; Adamson, J.; Parr, T.; Baxter, R.; Huntley, B. Characterising inter-annual variation in the spatial pattern of thermal microclimate in a UK upland using a combined empirical–physical model. *Agric. For. Meteorol.* **2010**, *150*, 12–19. <https://doi.org/10.1016/j.agrformet.2009.07.014>.

32. Strauss, S. An ill wind: the Foehn in Leukerbad and beyond. *J. R. Anthropol. Inst.* **2007**, *13*, S165–S181. <https://doi.org/10.1111/j.1467-9655.2007.00406.x>.

33. Kochanski, A.K.; Jenkins, M.A.; Mandel, J.; Beezley, J.D.; Krueger, S.K. Real time simulation of 2007 Santa Ana fires. *For. Ecol. Manage.* **2013**, *294*, 136–149. <https://doi.org/10.1016/j.foreco.2012.12.014>.

34. Raphael, M.N. The Santa Ana Winds of California. *Earth Interact.* **2003**, *7*, 1–13. [https://doi.org/10.1175/1087-3562\(2003\)007<0001:TSAWOC>2.0.CO;2](https://doi.org/10.1175/1087-3562(2003)007<0001:TSAWOC>2.0.CO;2).

35. Seydi, S.T. Assessment of the January 2025 Los Angeles County wildfires: A multi-modal analysis of impact, response, and population exposure. *arXiv [eess.SP]* **2025**, [[arXiv:eess.SP/2501.17880](https://arxiv.org/abs/2501.17880)].

36. Schultz, D.; Steenburgh, W. Understanding Utah Winter Storms. *Bull. Am. Meteorol. Soc.* **2002**, pp. 189–210.

37. Steenburgh, W.; Halvorson, S.F.; Onton, D.J. Climatology of Lake-Effect Snowstorms of the Great Salt Lake. *Mon. Weather Rev.* **2000**, *128*, 709–727. [https://doi.org/10.1175/1520-0493\(2000\)128<0709:COLESO>2.0.CO;2](https://doi.org/10.1175/1520-0493(2000)128<0709:COLESO>2.0.CO;2).

38. Lawson, J.; Horel, J. Analysis of the 1 December 2011 Wasatch Downslope Windstorm. *Weather Forecast.* **2015**, *30*, 115–135, [<https://dx.doi.org/10.1175/WAF-D-13-00120.1>]. <https://doi.org/10.1175/WAF-D-13-00120.1>.

39. Bestul, K.A. Analysis, Forecast Skill, and Predictability of Downslope Wind Events Along the Wasatch Front **2023**.

40. Steenburgh, W.J.; Alcott, T.I. Secrets of the “greatest snow on earth”. *Bull. Am. Meteorol. Soc.* **2008**, *89*, 1285–1294. <https://doi.org/10.1175/2008bams2576.1>.

41. Yang, S.; Hao, X.; Li, N.; Liao, H.; Li, J. Seasonal prediction of ozone pollution in central-east China using machine learning. *Aerosol Sci. Eng.* **2025**, pp. 1–9. <https://doi.org/10.1007/s41810-025-00310-7>.

42. Ghan, S.J.; Shippert, T.; Fox, J. Physically based global downscaling: Regional evaluation. *J. Clim.* **2006**, *19*, 429–445. <https://doi.org/10.1175/jcli3622.1>.

43. Pomeroy, J.; Gray, D.; Landine, P. The Prairie Blowing Snow Model: characteristics, validation, operation. *Journal of Hydrology* **1993**, *144*, 165–192. [https://doi.org/10.1016/0022-1694\(93\)90171-5](https://doi.org/10.1016/0022-1694(93)90171-5).

44. Essery, R.; Li, L.; Pomeroy, J. A distributed model of blowing snow over complex terrain. *Hydrological Processes* **1999**, *13*, 2423–2438. [https://doi.org/10.1002/\(SICI\)1099-1085\(199910\)13:14/15<2423::AID-HYP53>3.0.CO;2-U](https://doi.org/10.1002/(SICI)1099-1085(199910)13:14/15<2423::AID-HYP53>3.0.CO;2-U).

45. Franz, K.J.; Hogue, T.S.; Sorooshian, S. Operational snow modeling: Addressing the challenges of an energy balance model for National Weather Service forecasts. *J. Hydrol. (Amst.)* **2008**, *360*, 48–66. <https://doi.org/10.1016/j.jhydrol.2008.07.013>.

46. Franz, K.J.; Hogue, T.S.; Sorooshian, S. Snow model verification using ensemble prediction and operational benchmarks. *J. Hydrometeorol.* **2008**, *9*, 1402–1415. <https://doi.org/10.1175/2008jhm995.1>.

47. Veals, P.G.; Pletcher, M.; Schwartz, A.J.; Chase, R.J.; Harnos, K.; Correia, J.; Wessler, M.E.; Steenburgh, W.J. Predicting snow-to-liquid ratio in the mountains of the western United States. *Weather Forecast.* **2025**, *-1*. <https://doi.org/10.1175/waf-d-24-0233.1>.

48. Bormann, K.J.; Westra, S.; Evans, J.P.; McCabe, M.F. Spatial and temporal variability in seasonal snow density. *J. Hydrol. (Amst.)* **2013**, *484*, 63–73. <https://doi.org/10.1016/j.jhydrol.2013.01.032>.

49. Fobes, C.B. Snowfall in Maine. *Geogr. Rev.* **1942**, *32*, 245. <https://doi.org/10.2307/210273>.

50. Kusaka, H.; Suzuki, N.; Yabe, M.; Kobayashi, H. The snow-shadow effect of Sado Island on Niigata City and the coastal plain. *Atmos. Sci. Lett.* **2023**, *24*. <https://doi.org/10.1002/asl.1182>.

51. Ikeda, S.; Wakabayashi, R.; Izumi, K.; Kawashima, K. Study of snow climate in the Japanese Alps: Comparison to snow climate in North America. *Cold Reg. Sci. Technol.* **2009**, *59*, 119–125. <https://doi.org/10.1016/j.coldregions.2009.09.004>.

52. Veals, P.G.; Steenburgh, W.J.; Nakai, S.; Yamaguchi, S. Factors affecting the inland and orographic enhancement of sea-effect snowfall in the Hokuriku region of Japan. *Mon. Weather Rev.* **2019**, *147*, 3121–3143. <https://doi.org/10.1175/mwr-d-19-0007.1>.

53. de Gouw, J.A.; Veefkind, J.P.; Roosenbrand, E.; Dix, B.; Lin, J.C.; Landgraf, J.; Levelt, P.F. Daily satellite observations of methane from oil and gas production regions in the United States. *Sci. Rep.* **2020**, *10*, 1379. <https://doi.org/10.1038/s41598-020-57678-4>.

54. Zoogman, P.; Jacob, D.J.; Chance, K.; Liu, X.; Lin, M.; Fiore, A.; Travis, K. Monitoring high-ozone events in the US Intermountain West using TEMPO geostationary satellite observations. *Atmos. Chem. Phys.* **2014**, *14*, 6261–6271.

55. Jellis, D.; Bowman, K.; Rapp, A. Lifetimes of overshooting convective events using high-frequency gridded radar composites. *Mon. Weather Rev.* **2023**. <https://doi.org/10.1175/mwr-d-23-0032.1>.

56. Carbone, R.E.; Tuttle, J.D.; Ahijevych, D.A.; Trier, S.B. Inferences of Predictability Associated with Warm Season Precipitation Episodes. *J. Atmos. Sci.* **2002**, *59*, 2033–2056, [[http://dx.doi.org/10.1175/1520-0469\(2002\)059<2033:IOPAWW>2.0.CO;2](http://dx.doi.org/10.1175/1520-0469(2002)059<2033:IOPAWW>2.0.CO;2)]. [https://doi.org/10.1175/1520-0469\(2002\)059<2033:IOPAWW>2.0.CO;2](https://doi.org/10.1175/1520-0469(2002)059<2033:IOPAWW>2.0.CO;2).

57. De Pondeca, M.S.F.V.; Manikin, G.S.; DiMego, G.; Benjamin, S.G.; Parrish, D.F.; James Purser, R.; Wu, W.S.; Horel, J.D.; Myrick, D.T.; Lin, Y.; et al. The Real-Time Mesoscale Analysis at NOAA's National Centers for Environmental Prediction: Current Status and Development. *Weather and Forecasting* **2011**, *26*, 593–612. <https://doi.org/10.1175/WAF-D-10-05037.1>.

58. Morris, M.T.; Carley, J.R.; Colón, E.; Gibbs, A.; De Pondeca, M.S.F.V.; Levine, S. A quality assessment of the Real-Time Mesoscale Analysis (RTMA) for aviation. *Weather Forecast.* **2020**, *35*, 977–996. <https://doi.org/10.1175/waf-d-19-0201.1>.

59. Tyndall, D.; Horel, J. Impacts of Mesonet Observations on Meteorological Surface Analyses. *Weather and Forecasting* **2013**, *28*, 254–269. <https://doi.org/10.1175/WAF-D-12-00027.1>.

60. Knopfmeier, K.; Stensrud, D. Influence of mesonet observations on the accuracy of surface analyses generated by an ensemble Kalman filter. *Weather and Forecasting* **2013**, *28*, 815–841. <https://doi.org/10.1175/WAF-D-12-00078.1>.

61. Ancell, B.C.; Mass, C.F.; Cook, K.; Colman, B. Comparison of surface wind and temperature analyses from an ensemble Kalman filter and the NWS Real-Time Mesoscale Analysis system. *Weather Forecast.* **2014**, *29*, 1058–1075. <https://doi.org/10.1175/waf-d-13-00139.1>.

62. Nelson, B.R.; Prat, O.P.; Seo, D.J.; Habib, E. Assessment and Implications of NCEP Stage IV Quantitative Precipitation Estimates for Product Intercomparisons. *Weather Forecast.* **2016**, *31*, 371–394. <https://doi.org/10.1175/WAF-D-14-00112.1>.

63. Pearson, R.K.; Neuvo, Y.; Astola, J.; Gabbouj, M. Generalized Hampel Filters. *EURASIP J. Adv. Signal Process.* **2016**, *2016*, 1–18. <https://doi.org/10.1186/s13634-016-0383-6>.

64. Lyman, S.; Jones, C.; Lawson, J.R.; Mansfield, M.; David, L.; O'Neil, T.; Holmes, B. Bingham Center 2023 Annual Report. Technical report, 2023. <https://doi.org/10.5281/zenodo.13999274>.

65. Holder, J.; Jordan, J.; Johnson, K.; Akinremi, A.; Roberts-Semple, D. Using low-cost sensing technology to assess ambient and indoor fine particulate matter concentrations in New York during the COVID-19 lockdown. *Air (Basel)* **2023**, *1*, 196–206. <https://doi.org/10.3390/air1030015>.

66. Ancell, B.; Hakim, G.J. Comparing Adjoint- and Ensemble-Sensitivity Analysis with Applications to Observation Targeting. *Mon. Wea. Rev.* **2007**, *135*, 4117–4134, [<http://journals.ametsoc.org/doi/pdf/10.1175/2007MWR1904.1>]. <https://doi.org/10.1175/2007MWR1904.1>.

67. Mansfield, M.L.; Hall, C.F. Statistical analysis of winter ozone events. *Air Qual. Atmos. Health* **2013**, *6*, 687–699. <https://doi.org/10.1007/s11869-013-0204-0>.

68. Doviak, R.J.; Zrnic, D.S.; Schotland, R.M. Doppler radar and weather observations. *Appl. Opt.* **1994**, *33*, 4531.

Disclaimer/Publisher's Note: The statements, opinions and data contained in all publications are solely those of the individual author(s) and contributor(s) and not of MDPI and/or the editor(s). MDPI and/or the editor(s) disclaim responsibility for any injury to people or property resulting from any ideas, methods, instructions or products referred to in the content.